View metadata, citation and similar papers at core.ac.uk
brought to you by CORE
provided by Digital.CSIC

Submitted to ADVANCED MATERIALS
DOI: 10.1002/adma.((please add manuscript number))

Hybrid magnetic/superconducting materials obtained by insertion of a single-molecule magnet into TaS_2 layers

By *Eugenio Coronado*, Carlos Martí-Gastaldo, Efrén Navarro-Moratalla,* Enrique Burzurí, *Agustín Camón, and Fernando Luis*

[*] Prof. E. Coronado, Dr. C. Martí-Gastaldo, E. Navarro-Moratalla
Instituto de Ciencia Molecular (ICMol))
Universidad de Valencia
Catedrático José Beltrán Martínez nº 2, 46980, Paterna (Spain)
E-mail: *eugenio.coronado@uv.es*

Dr. C. Martí-Gastaldo (*current address*)
Department of Chemistry
University of Liverpool
Crown Street, L697ZD, Liverpool (UK)

Dr E. Burzurí, Prof. A. Camón, Prof. F. Luis
Instituto de Ciencia de Materiales de Aragón (ICMA/CSIC)
Universidad de Zaragoza
C/ Pedro Cerbuna 12, 50009, Zaragoza (Spain)

Keywords: hybrid multifunctional materials, single molecule magnets (SMMs), layered superconductors, tantalum disulphide

Among the hot topics in materials chemistry, the design of novel materials in which two or more physical properties of interest can be rationally combined into the same solid is currently attracting important attention. With this regard, the versatility of the molecular building-block approach, which relies on the combination of different molecular entities carrying specific functionalities into an extended molecule-based solid, has proven to be a very fruitful synthetic route.[1-5]

A more unusual approach is that relying on the combination of molecular materials with solid-state extended hosts. Though less exploited, this route has already permitted the organized assembly of functional molecules into mesoporous frameworks,[6] or more recently, to restrict the growth of cyanide-bridged or oxalate-based molecular magnets in two-dimensions within layered double hydroxides (LDH).[7] In this context, the exfoliation of layered inorganic solids, defined as their segregation into single entities through soft

chemistry methods,[8] can be regarded as a versatile alternative for the combination of such solid-state host with a variety of functional molecules. Once exfoliated in organic solvents, these lamellae constitute stable suspensions of sheets that may retain the physical properties of the pristine bulk materials, hence enabling the design of new advanced hybrid materials or nanoelectronic devices.[9, 10] In the past, the combination of conductivity and magnetic bi-stability has been sought for using the molecular building block approach.[11] However, only very recently has the present strategy been exploited for the design and synthesis of superconducting-ferromagnetic materials.[12]

Herein we use the hybrid solid-state/molecular route as a tool for the design of layered superconductors containing single molecule magnets (SMM). Besides the natural interest linked to the organization of magnetic clusters within the interlamellar space offered by a layered host, we here address the prospective physical implications which might result from the presence of magnetic sites in close proximity with a superconducting lattice. We aimed to study the mutual influence between these two compounds, i.e. the effect that the large diamagnetism of the superconductor (SC) below its transition temperature might have on the relaxation dynamics of the SMM cluster and, at the same time, the effect that the large spins of the SMM have on the superconducting properties of a Type-II layered SC. Finally, the controlled integration of SMMs in direct contact with 2D superconducting layers might contribute to the development of hybrid architectures for sensing and manipulating mesoscopic spins, with possible applications in the field of quantum information.[13]

Among the vast library of layered inorganic solids available, we focused on a classical system: tantalum disulphide, TaS_2.[14] This compound belongs to a general family of metal dichalcogenides (MX_2 M= Ti, Mo, Nb, Ta; X= S, Se, Te), which has been extensively studied from the early seventies, when Gamble *et al.* observed low-temperature superconductivity in parent TaS_2 and related pyridine-intercalated materials.[15] From a structural point of view,

tantalum disulphide can be considered as a layered material built from the stacking of neutral weakly interacting 2D TaS_2 layers, composed by trigonal prismatic Ta (IV) ions covalently bonded to sulphur ions distributed above and below the plane defined by the metal atoms. The relative stacking orientation of these layers and the coordination symmetry of the metal atom within them have turned out to be very important parameters, dramatically affecting the physical properties of the resulting polymorphs.[16] When immersed in sodium hydroxide aqueous solutions, tantalum disulphide undergoes topotactic reduction reaction producing the intercalation compound: $Na_x[TaS_2]$ (x= +0.24 – +0.33).[17] During this process, electrons are transferred from the reducing agent to the neutral TaS_2 layers, this having two major consequences: on the one hand, the layers become negatively charged and, on the other, the critical temperature (T_{SC}) below which superconductivity is observed increases from 0.15 K, for the neutral pristine tantalum disulphide, up to 4.5 K.[17] Moreover, the intercalation of guest species promotes the expansion of the interlayer space thereby weakening the interlayer interactions. This feature can be profited from to exfoliate the intercalated material into stable emulsions of anionic superconducting and highly anisotropic $[TaS_2]^{-0.33}$ nanosheets.[18] A direct combination of the intrinsic 2D superconductivity provided by the $[TaS_2]^{-0.33}$ anionic layers with the magnetic features of cationic single molecule magnets (SMMs) may now be envisioned by sheer electrostatic re-stacking of a layered solid-state/molecular material.

As SMM cationic unit, we chose the Mn_4 polynuclear cluster: $[Mn_4(OAc)_2(pdmH)_6]^{2+}$ (pdmH = deprotonated pyridine-2,6-dimethanol; $C_5H_4NO_2$).[19] This system is composed of a central tetramer of $(Mn^{2+})_2/(Mn^{3+})_2$ ions bridged through oxo (O^{2-}) ligands. It exhibits a ground spin state S = 8 ± 1 and superparamagnetic blocking below 2.5 K. Regardless of their higher blocking temperatures, we discarded the employment of other unimolecular magnets belonging to the Mn_{12} family because of their poor chemical stability.[20] Oppositely, the chemical robustness of the Mn_4 complex has been already demonstrated through its use in the design of several magnetic topologies.[21]

The synthetic route started with the ceramic combination of S and Ta flours, affording µ-crystalline samples of TaS_2 (**1**) as previously described in the literature.[15] A survey of different synthetic conditions (SI1) and their corresponding distinct crystallographic phases and sample morphologies depicted the importance of controlling the precursor polytype in the following Na^+ intercalation step. Only a 2H/6R TaS_2 phase with morphologically regular hexagonal µ-crystallites of around 30-50 µm wide underwent successful and reproducible intercalation resulting in a pure δ-2H-$Na_{0.33}[TaS_2]$ (**2**) non-stoichiometric phase where approximately one third of the Ta (IV) atoms had been reduced to Ta (III). Though the precise nature of the reduction mechanism remains uncertain, a likely explanation points at the presence of reducing S^{2-} ions in the medium, arising from the residual hydrolysis of pristine TaS_2 slabs.[17a] The final step in the synthesis of the hybrid involved the exchange of the Na^+ intercalated atoms by $[Mn_4]^{2+}$ entities in a delamination/flocculation process. A careful addition of an acetonitrile solution containing a fixed concentration of $[Mn_4(OAc)_2(pdmH)_6]^{2+}$ cations (**3**) to a freshly prepared emulsion of $[TaS_2]^{-0.3}$ 2D sheets triggered attractive electrostatic interactions between the oppositely charged species coexisting in solution and drove the assembly of the new layered hybrid superstructure of formula $[TaS_2][Mn_4(OAc)_2(pdmH)_6]_{0.15}$ (**4**). Worthwhile mentioning is that in order to discard a mere co-precipitation of both components, a range of $[Mn_4]^{2+}$: $[TaS_2]^{-0.33}$ non-equivalent concentration ratios were explored all of which lead to homogeneous phases with the same stoichiometry within experimental error as analysed by electron microscopy techniques (SI7).

X-Ray Photoelectron Spectroscopy (XPS) experiments were performed and provided evidence for the presence of Mn_4 clusters with binding energies that are in good agreement with the expected bonding states. The Mn $2p_{3/2}$ (up) and Mn 3s (down) signals exhibited by the hybrid **4** are in good agreement with the data collected for **3**. Concerning oxidation states, this provides a strong indication of the presence of the unaltered Mn_4 SMM core within the TaS_2 (SI12).

Direct comparison between the X-Ray diffraction data collected from ground samples of the starting materials (**2**, **3**) and the restacked hybrid (**4**), confirms that the diffraction profile observed for the latter is not merely a superposition of the XRPD profiles of the precursors, supporting the generation of a novel lamellae crystalline phase in the solid state from the combination of the ionic nanosheets in solution (**Figure 1**). Because of the protocol employed in its re-assembling, **4** presents a bigger number of stacking defects and overall disorder than the starting components, as denoted by the weaker intensity and broader profile of the reflection lines. These problems have generally hindered the determination of accurate structural models for intercalation complexes of layered dichalcogenides.[22] Still, two sharp intense diffraction peaks and a broader less intense one, which can be indexed as (*002*), (*003*) and (*004*) reflections by assuming a hexagonal unit cell, are observed at low angular values and permit estimating a *'c'* axis value of 19.76 Å. In contrast with the neutral host and the δ-Na^+-intercalated 2H polytypes (with basal spacing, *BS*=*c*/2, of 6.1 Å and 11.8 Å, respectively), this value suggests the formation of a 1H phase (*BS*=*c*) with an eclipsed packing of the TaS_2 slabs in the solid-state, result of their exfoliation and subsequent combination with the Mn_4 complex in solution. This stacking periodicity provides a *BS* of *ca.* 19.8 Å for **4**, in excellent agreement with the addition of the thicknesses of one TaS_2 layer (3.1 Å),[23] and the average size of the Mn_4 complex (*ca.* 15 Å in diameter assuming a spherical model).

The magnetization (see SI10 and SI11) and the magnetic dynamical susceptibility (**Figure 2**) performed on bulk powder samples of the hybrid material (**4**) clearly show the coexistence of a diamagnetic response, characteristic of the superconductivity, and a paramagnetic one, which can be attributed to the Mn_4 clusters. The AC susceptibility of **4** is dominated by the transition to the superconducting state at T_{SC} = 4.2 K, and is frequency independent above 2 K Nevertheless, though masked by the enormous diamagnetic susceptibility of the superconducting layers, a maximum is observed in the out-of-phase component, clearly

shifted to lower temperatures in comparison with the reference cluster **3.** This peak shows a frequency dependence which can be described with an Arrhenius law, indicating the existence of the slow and thermally activated magnetic relaxation typical of SMMs. The Arrhenius fit (recall Fig. 1) gives an activation energy of U / k_B = 10.4(4) K. This barrier value is lower than the one estimated for **3** and explains why the AC susceptibility of **4** hardly depends on frequency above 2 K. In fact, the activation energy of **4** is approximately a half of that estimated for the starting pure SMM material **3** (U / k_B = 20(1) K).[19] This suggests that the magnetic relaxation of Mn_4 clusters is strongly influenced by the presence of the superconducting host, becoming faster as the clusters are inserted in between TaS_2 layers. The change in the magnetic behaviour of Mn_4 clusters in the hybrid material is also confirmed by the hysteresis loops measured on **3** and **4** at very low temperatures (see SI10). At T = 0.35 K, the coercive field of the Mn_4 sample **3**, $\mu_0 H_C$ = 0.33 T, is three times larger than that of the hybrid material **4**, $\mu_0 H_C$ = 0.11(2) T.

This faster magnetic relaxation may arise from two possible scenarios: a change in the structure of magnetic energy levels of the molecular cluster, that is, of the magnetic anisotropy associated with the different environment; or, alternatively, a faster tunnelling rate associated with the screening of intermolecular dipolar interactions by the superconducting layers. Further measurements of the magnetic relaxation in the presence of strong DC fields ($H > H_{c1}$ for $[TaS_2]^{-0.33}$) were performed in order to discriminate amongst these two situations (SI9). When the external field becomes larger than the lower critical field of the superconducting $[TaS_2]^{-0.33}$ component (H_{c1}~ 170 Oe; see SI8) the interactions are no longer screened and the relaxation rate is mainly determined by the strength of the magnetic anisotropy. The data measured on **4** remain different from those measured on the reference sample **3** at all fields, even for H = 3000 Oe when it is clear that T_{SC} of the superconducting fraction becomes smaller than 1.8 K (SI9). Under these conditions the relaxation of the

clusters should not be affected by the superconductivity of TaS_2. Therefore, we must conclude that the magnetic anisotropy of Mn_4 clusters is greatly modified by their insertion into TaS_2 layers.

This assumption is additionally supported by comparing the specific heat data of compounds **3** and **4** (**Figure 3**). The specific heat of a magnetic material provides direct information on the structure of magnetic energy levels and thus enables to ascertain if important changes in the anisotropy parameters have occurred. The experimental data reflect that the Schottky anomaly in **4** is markedly lower and shifted towards lower temperatures, as compared with the anomaly measured for **3**. This confirms that the zero-field splitting associated with the magnetic anisotropy of Mn_4 clusters becomes smaller as they are inserted into TaS_2. It also suggests that the net molecular spin, which determines the number of energy levels populated at these temperatures and thus the magnetic entropy change, might also be lower in the latter sample. This is confirmed by magnetization isotherms recorded for **4** that attain $M \approx 3.5$ μ_B/Mn_4 cluster at 2 K and 5 T, which is clearly below the saturation magnetization of **3** (16 μ_B; SI11). From the susceptibility (Fig. 2), we estimate a ground state S = 4 for the clusters in **4**, that is, one half the value S = 8 found in the starting material **3**. A final remark concerning the specific heat profile of hybrid **4** is the absence of a well-defined lambda peak. This is once again typical of strongly two-dimensional superconducting materials as opposed to three-dimensional bulk superconductivity. The intrinsic two-dimensional nature of superconductivity in TaS_2 and TaS_2-intercalated materials make them posses a very high level of entropy above T_c, hence the maximum smears in such a way that is hardly observable.[24]

It is important to note that whilst the relaxation and/or the intrinsic magnetic properties of the Mn_4 clusters experience modifications once nested in between TaS_2 layers, the superconducting behaviour of the dichalcogenide layers remains at most unaltered (T_{SC} = 4.2 K found for **4** is rather close to T_{SC} = 4.5 K of the precursor material 2, and also the value of

B_{c1} seems to change little, as shown in SI11). Additional magnetic susceptibility experiments performed on oriented samples allow for the direct observation of the anisotropic properties of the material together with the coexistence of SMM (that dominates in the magnetization profile at high fields) and superconductivity (clearly visible at the low-field region in the magnetization data in SI13). A coparallel orientation of the pellet with the external applied field leads to maximum shielding whilst an orthogonal one reduces the Meissner response. This once again supports the idea of a robust two-dimensional superconductivity of the inorganic part of the hybrid that operates even in the case of drastic structural changes such as the one herein considered.[25]

In conclusion, the hybrid solid-state/molecular approach has been here employed for the synthesis of the first material combining superconductivity and SMM properties. Thus, we have shown that superconductivity and SMM behaviour coexist in this chemically engineered hybrid material. Interestingly, the magnetic behaviour of the Mn_4 clusters suffers large changes as they are inserted in between the TaS_2 layers. In particular, the magnetic anisotropy becomes weaker, leading to a faster magnetic relaxation, and the molecular spin becomes smaller. The synthesis of this new material represents the first successful attempt to insert a functional molecule into this class of layered chalcogenide superconductors. On the other hand, it extends the hybrid strategy that arises from the combination of molecule-based components with solid-state inorganic structures.[6, 7] It is also a natural extension of the very recent superconducting-ferromagnetic material, proving the versatility of the layered dichalcogenide strategy for the combination of superconductivity with other interesting properties.[12] Finally it is also suggested that, although the presence of Mn_4 clusters in between TaS_2 host layers does not seem to affect the superconducting bulk properties, these high spin clusters may act as a vortex pinning centres. Future studies will be devoted to analyse the vortex dynamics in these hybrid superconductors.

Experimental

Physical characterization. Metallic composition and particle morphology and dimensions of bulk samples were estimated by electron probe microanalysis (EPMA) performed in a Philips SEM XL30 equipped with an EDAX microprobe operated at 20 kV. Carbon, nitrogen and hydrogen contents were determined by microanalytical procedures using an EA 1110 CHNS-O Elemental Analyzer from CE Instruments. Infrared spectra were recorded in a FT-IR Nicolet 5700 spectrometer in the 4000-400 cm^{-1} range using powdered samples diluted in KBr pellets. Thermogravimetric analysis of all compounds were carried out with a Mettler Toledo TGA/SDTA 851 apparatus in the 25-800 ºC temperature range under a 10 $ºC.min^{-1}$ scan rate and an air flow of 30 $mL.min^{-1}$. Powder X-ray diffraction (PXRD) patterns were collected with a Siemens d-500 X-ray diffractometer (Cu-K_{α} radiation; λ_{α} = 1.5418 Å) equipped with a rotating anode D-max Rigaku operating at 80 mA and 45 kV. Samples were mounted on a flat sample plate with grease. Conventional magnetic characterization was carried out with a commercial MPMS-XL SQUID magnetometer, operating between 300 and 1.8 K. Hysteresis loops were measured between 350 mK and 7 K using a homemade micro-Hall magnetometer working in a ^{3}He refrigerator. The sample, mixed with Apiezon N grease to ensure thermalization at these very low temperatures, was deposited directly on the edge of one of the two Hall crosses. The ac susceptibility was also measured, from 333 Hz up to 13 kHz, using a home-built mutual inductance susceptometer thermally anchored to the mixing chamber of a ^{3}He-^{4}He dilution refrigerator, which gives access to temperatures ranging from 0.09 K up to 3.5 K. A lock-in amplifier amplifies the voltages arising from in-phase and out-of-phase magnetic signals. The errors involved in the determination of the output signal's phase have been determined separately by measuring a reference signal and are found to be smaller than 0.01 deg. for any frequency. Finally, specific heat data were also measured between 350 mK and 20 K on compact pellets using a commercial Physical Properties Measurement System (PPMS).

General synthetic remarks. All chemicals and solvents employed were of commercially available grade and were used without any previous purification. $[Mn_4(OAc)_2(pdmH)_6](ClO_4)_2$ **3** (pdmH = deprotonated pyridine-2,6-dimethanol; $C_5H_4NO_2$) was synthesized according to the method previously described by Yoo *et al.* [19].

Synthesis of TaS_2 (**1**). Stoichiometric ratios of tantalum (2.422 g) and sulphur (0.858 g) were exhaustively mixed with the help of pestle and mortar and put into a purged quartz ampoule (length=30 cm; internal diameter=15 mm). The system was transferred to a ceramic furnace and subjected to the following thermal treatment: 1) Heating from room temperature up to 900º C at 5º C.min^{-1}; 2) Constant heating at 900º during nine days; 3) Cooling down to room temperature. The resulting glittering black solid was separated by hand from traces of non-consumed metallic sulphur and stored under Ar atmosphere.

Synthesis of δ-$Na_{0.33}[TaS_2]\cdot 1.9H_2O$ (**2**). 20 mL of a freshly prepared aqueous solution of NaOH 50 mM (40 mg dissolved in 20 mL of deionized water; pH = 12.7) were added onto 450 mg of free-flowing TaS_2(s). The mixture was mechanically stirred during 2 hrs in a gentle manner. The Na^+-intercalated solid was recovered by *in vacuo* filtration of the resulting yellowish slurry and washed thoroughly with a few millilitres of ultrapure milli-Q water. Finally, the moist grey powder was dried overnight under static vacuum over silica gel and the resulting glittering dark metallic solid stored under Ar atmosphere.

Synthesis of $[Mn_4(OAc)_2(pdmH)_6]_{0.15}[TaS_2]$ (**4**). Typically, 222 mg of $Na_{0.33}TaS_2$ black powder (0.88 mmol) were suspended in 150 mL of a 1:1 (v/v) mixture of ultrapure Milli-Q water and N-methylformamide. At this stage, sedimentation of the solid material occurred at once, was the suspension left to stand. The $Na_{0.33}TaS_2$ exfoliation process was then carried out in three successive steps: 1) 3 minutes of mechanical stirring; 2) 20 minutes of ultrasonic bath treatment; 3) 5 extra minutes of mechanical stirring. Upon completion of the exfoliation step the suspension had attained stability as well as a remarkable 'pearl effect' if stirred. The final

flocculation stage involved dropwise addition of 75 mL of a 2 mM $[Mn_4(OAc)_2(pdmH)_6](ClO_4)_2$ solution (0.15 mmol) in acetonitrile, over the delaminated $Na_{0.33}TaS_2$ stable suspension under gentle stirring. The addition rate was controlled via Ar pressure and the use of cannula transferring material. Allowing the slurry to stir for 20 minutes, the resulting suspension had lost stability and sedimented readily at the bottom of the flask once left to stand still. The yellowish supernatant was decanted off. The recovered black solid was then washed thrice by re-suspension-decantation with 100 mL fresh acetonitrile. *In vacuo* drying of the material yielded a glittering grey powder best preserved under Ar atmosphere.

Acknowledgements

Financial support from the EU (MolSpinQIP) and the ERC (SPINMOL Advanced Grant to EC), the Spanish Ministerio de Ciencia e Innovación (Project Consolider-Ingenio in Molecular Nanoscience and projects MAT2007-61584, MAT2009-13977-C03, and CTQ-2008-06720, co-financed by FEDER) and the Generalitat Valenciana (Prometeo Program) are gratefully acknowledged. ENM thanks the Spanish Ministerio de Ciencia too for a FPU grant. CMG thanks the EU for a Marie Curie Fellowship (IEF-253369). We also acknowledge J. M. Martínez for magnetic measurements. ((Supporting Information is available online from Wiley InterScience or from the author)).

Received: ((will be filled in by the editorial staff))
Revised: ((will be filled in by the editorial staff))
Published online: ((will be filled in by the editorial staff))

_[1] E. Coronado, J. R. Galán-Mascarós, C. J. Gómez-García, V. Laukhin, *Nature* **2000**, *408*, 447-449.

_[2] a) O. Sato, T. Iyoda, A. Fujishima, K. Hashimoto, *Science* **1996**, *272*, 704- 705. (b) E. Coronado, M. C. Giménez-López, T. Korzeniak, G. Levchenko, F. M. Romero, A. Segura, V. García-Baonza, J. C. Cezar, F. M. F. de Groot, A. Milner, M. Paz-Pasternak, *J. Am. Chem. Soc.* **2008**, *130*, 15519-15532.

_[3] a) M. Minguet, D. Luneau, E. Lhotel, V. Villar, C. Paulsen, D. B. Amabilino, J. Veciana, *Angew. Chem. Int. Ed.* **2002**, *41*, 586-589. (b) K. Inoue, K. Kikuchi, M. Ohba, H. Okawa, *Angew. Chem. Int. Ed.* **2003**, *42*, 4810–4813. (c) C. Train, R. Gheorge, V. Krstic, L.-M. Chamoreau, N. S. Ovanesyan, G. L. J. A. Rikken, M. Gruselle, M. Verdaguer, *Nat. Mater.* **2008**, *7*, 729-734.

_[4] a) H. Cui, Z. Wang, K. Takahashi, Y. Okano, H. Kobayashi and A. Kobayashi, *J. Am. Chem. Soc.* **2006**, *128*, 15074-15075. (b) G. Rogez, N. Viart, M. Drillon, *Angew. Chem. Int. Ed.* **2010**, *49*, 1921-1923.

_[5] a) S. Floquet, S. Salunke, M. L. Boillot, R. Clément, F. Varret, K. Boukheddaden, E. Rivière, *Chem. Mater.* **2002**, *14*, 4164–4171. (b) S. Floquet, M. C. Muñoz, E. Rivière, R. Clément, J. P. Audière, M. L. Boillot, *New J. Chem.* **2004**, *28*, 535-541. (c) M. Clemente-León, E. Coronado, M. C. Giménez-López, A. Soriano-Portillo, J. C. Waerenborgh, F. S. Delgado, C. Ruiz-Pérez, *Inorg. Chem.* **2008**, *47*, 9111-9120.

_[6] a) C. A. Strassert, M. Otter, R. Q. Albuquerque, A. Höne, Y. Vida, B. Maier, L. De Cola, *Angew. Chem. Int. Ed.* **2009**, *48*, 7928-7931. (b) Z. Popovic, M. Busby, S. Huber, G. Calzaferri, L. De Cola, *Angew. Chem. Int. Ed.* **2007**, *46*, 8898-8902.

_[7] a) E. Coronado, C. Martí-Gastaldo, E. Navarro-Moratalla, A. Ribera, *Inorg. Chem.* **2010**, *49*, 1313-1315. (b) E. Coronado, C. Martí-Gastaldo, E. Navarro-Moratalla, A. Ribera, J.R. Galán-Mascarós, *J. Mater. Chem.* **2010**, *20 (42)*, 9476-9483

_[8] a) A. Jacobson, *J. Mater. Sci. Forum* **1994**, *1*, 152-153 (b) T. Sasaki, M. Watanabe, H. Hashizume, H. Yamada, H. Nakazawa, *J. Am. Chem. Soc.* **1996**, *118*, 8329-8335; (c) R. Abe, K. Shinohara, A. Tanaka, M. Hara, J. N. Kondo, K. Domen, *Chem. Mater.* **1997**, *9*, 2179-2184; d) R. E. Schaak, T. E. Mallouk, *Chem. Mater.* **2000**, *12*, 2513-2516.

_[9] a) D. M. Kaschak, J. T. Lean, C. C. Waraksa, G. B. Saupe, H. Usami, T. E. Mallouk, *J. Am. Chem. Soc.* **1999**, *121*, 3435-3445. (b) M. Osada, Y. Ebina, K. Takada, T. Sasaki, *Adv. Mater.* **2006**, *18*, 1023-1027.

_[10] B. Radisavljevic, A. Radenovic, J. Brivio, V. Giacometti, A. Kis, *Nature Nanotechnology* **2011**, *6 (3)*, 147-150.

_[11] H. Hiraga, H. Miyasaka, K. Nakata, T. Kajiwara, S. Takaishi, Y. Oshima, H. Nojiri, M. Yamashita, *Inorg. Chem.* **2007**, *46 (23)*, 9661-9671.

_[12] E. Coronado, C. Martí-Gastaldo, E. Navarro-Moratalla, A. Ribera, S. J. Blundell, P. J. Baker, *Nat. Chem.* **2010**, *2*, 1031-1036.

_[13] A. Imamoglu, *Phys. Rev. Lett.* **2009**, *102*, 083602 (1-4).

_[14] F. Jellinek, *Journal of The Less-Common Metals* **1962**, *4* (1), 9-15.

_[15] F. R. Gamble, F. DiSalvo, R. Klemm, T. Geballe, *Science* **1970**, *168*, 568-570.

_[16] R. H. Friend, A. D.Yoffe, *Advances in Physics* **1987**, *36 (1)*,1-94. *Section 3*.

_[17] Depending on the specific conditions of the experiment, *x* may be variable. For detailed studies see: (a) W. Biberacher, A. Lerf, F. Buheitel, T. Butz, A. Hubler, *Mat. Res. Bull.* **1982**, *17*, 633-640. (b) R. Schollhorn, E. Sick, A. Lerf, *Mat. Res. Bull.* **1975**, *10*, 1005-1012.

_[18] L. F. Nazar, A. J. Jacobson, *J. Mater. Chem.* **1994**, *4*, 1419-1425.

_[19] J. Yoo, E. K. Brechin, A. Yamaguchi, M. Nakano, J. C. Huffman, A. L. Maniero, L.-C. Brunel, K. Awaga, H. Ishimoto, G. Christou, D. N. Hendrickson, *Inorg. Chem.* **2000**, *39*, 3615-3623.

_[20] M. Mannini, F. Pineider, P. Sainctavit, L. Joly, A. Fraile-Rodríguez, M-A. Arrio, C. Cartier dit Moulin, W. Wernsdorfer, A. Cornia, D. Gatteschi, R. Sessoli, *Adv. Mater.* **2009,** *21 (2)*, 67-171.

_[21] a) H. Miyasaka, K. Nakata, K. Sugiura, M. Yamashita, R. Clerac, *Angew. Chem. Ed.* **2004**, *43*, 707. (b) H. Miyasaka, K. Nakata, L. Lecren, C. Coulon, Y. Nakazawa, T. Fujisaki, K.-I. Sugiura, M. Yamashita, R. Clérac, *J. Am. Chem. Soc.* **2006**, *128 (11)*, 3770-3783.

_[22] H. V. Wong, J. S. O. Evans, S. Barlow, S. J. Mason, D. O'Hare, *Inorg. Chem.* **1994**, *33*, 5515.

_[23] a) D. W. Bruce, D. O'Hare, *Inorganic Materials*, Ed.: John Wiley & Sons, **1997**. (b) A. Meetsma, G. A. Wiegers, R. J. Haange, J. L. de Boer, *Acta Cryst.* **1990**, *C46*, 1598-1599.

_[24] a) T. Geballe, A. Menth, F. Di Salvo, F. Gamble, *Phys. Rev. Lett.* **1971**, *27*, 314–316. (b) J. A. Benda, *Phys. Rev. B* **1974**, *10*, 1409–1420. (c) S. Meyer, R. Howard, G. Stewart, J. V. Acrivos, T. H. Geballe, *J. Chem. Phys.* **1975**, *62 (11)*, 4411-4419. (d) A. Schlicht, M. Schwenker, W. Biberacher, *A. Lerf, J. Phys. Chem. B* **2002**, *105*, 4867–4871.

_[25] R. H. Friend, A. D.Yoffe, *Advances in Physics* **1987**, *36 (1)*,1-94. *Section 7.3*.

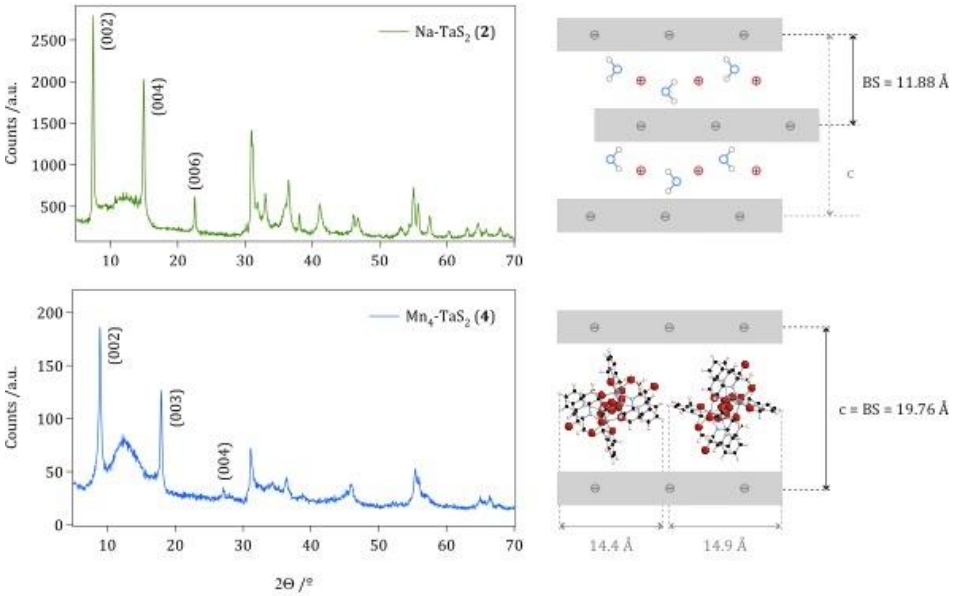

Figure 1. Structural model ascribed to the powder patterns observed for δ-2H-$Na_{0.33}[TaS_2]$ (**2**, *top*) and $[Mn_4(OAc)_2(pdmH)_6]_{0.15}[TaS_2]$ (**4**, bottom).

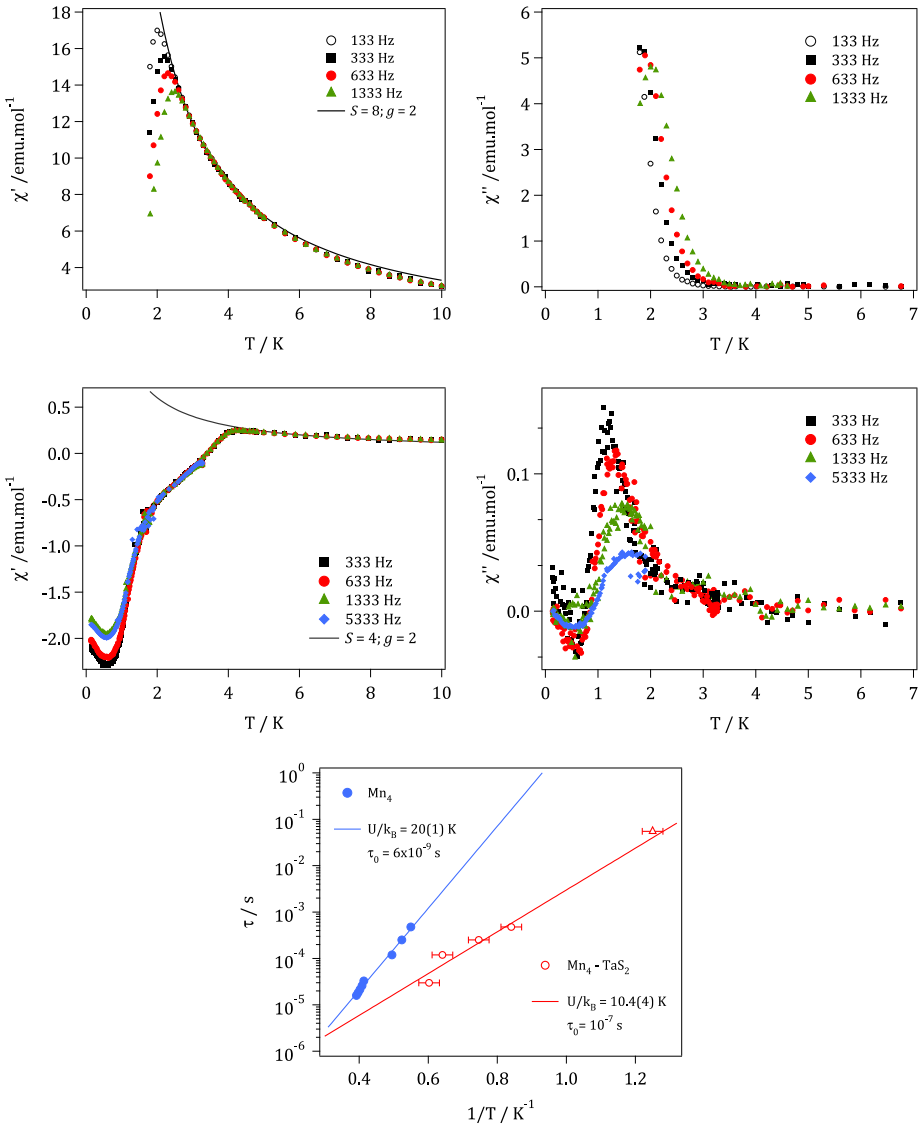

Figure 2. AC magnetic study of the SMM material **3** (top panels) and of the hybrid material **4** (bottom panels). *Left*: In-phase susceptibility component. The solid lines show the predicted susceptibility of anisotropic spins $\chi = N_A(gS\mu_B)^2/3k_B(T-\theta)$ for two different values of g and S. The Weiss temperature θ = 0.3 K for **3** and ≈ 0 for **4**. *Right*: Out-of-phase susceptibility component. *Bottom*: Arrhenius plot of **3** (blue) and **4** (red) extracted from out-of-phase AC signal (the triangular marker of the plot for **4** represents a data point estimated from the temperature dependence of the remanent magnetization measured below 1 K).

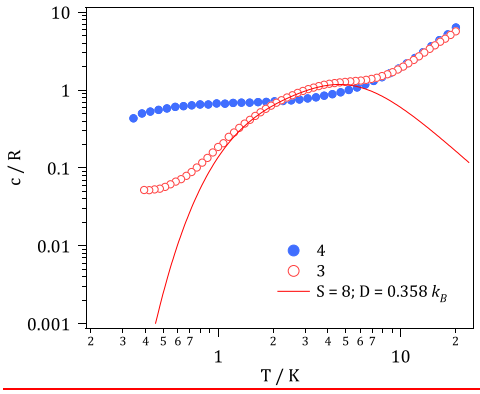

Figure 3. Specific heat data for the molecular compound **3** and the hybrid material **4** measured as a function of temperature under zero applied field and the calculated profile for Mn_4 cluster (S = 8 and D = 0.358 k_B). To allow a direct comparison between the two, the specific heat is given per mol of Mn_4 clusters in the two samples.

Submitted to ADVANCED MATERIALS

The table of contents entry:

A material in which superconducting and magnetic bistable properties coexist is synthesized by the intercalation of single–molecule magnets into the layered structure of a group V metal dichalcogenide. The coexistence and synergy of both functionalities is addressed. A molecule-based/solid-state hybrid strategy is here employed, proving as a promising technique for the future combination of superconductivity with different molecule-intrinsic functionalities.

Keyword (see list): hybrid multifunctional materials, single molecule magnets (SMMs), layered superconductors, tantalum disulphide.

Eugenio Coronado*, Carlos Martí-Gastaldo, Efrén Navarro-Moratalla, Enrique Burzurí, Agustín Camón, and Fernando Luis

Hybrid magnetic/superconducting materials obtained by insertion of a single-molecule magnet into TaS_2 layers

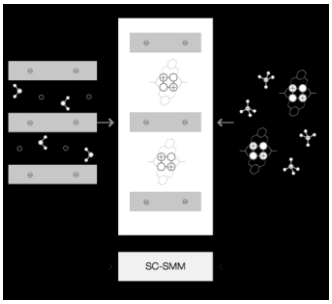

Submitted to ADVANCED MATERIALS

Multifunctional Hybrid Materials combining Superconductivity and Magnetic Bistability

Eugenio Coronado, Carlos Martí-Gastaldo, Efrén Navarro-Moratalla, Enrique Burzurí, Agustín Camón, and Fernando Luis*

[*] Prof. E. Coronado
Dr. C. Martí-Gastaldo, E. Navarro-Moratalla
Universidad de Valencia (ICMol)
Polígono de la Coma s/n, 46980, Paterna (Spain)
E-mail: eugenio.coronado@uv.es

Prof. A. Camón, Prof. F. Luis, E. Urbizu
Instituto de Ciencia de Materiales de Aragón (ICAM/CSIC)
Universidad de Zaragoza
C/ Pedro Cerbuna 12, 50009, Zaragoza (Spain)

SI 1. TaS_2 synthetic conditions.

(*Top*) Table with a sample of synthesis conditions surveyed including conditions of precursor material **1** (*Bottom*) XRPD corresponding to reaction conditions described in preceding table.

	Plateau /ºC	Δ rate /ºC min^{-1}	Cooling time /hrs	Load fashion
1	900	5	3	Evenly spread
A	900	4.5	10	Evenly spread
B	950	1	48	Tightly packed
C	900	4.5	10	Evenly spread
D	950	0.2	10	Evenly spread
E	950	1	48	Evenly spread
F	950	0.2	10	Evenly spread

NB: A constant plateau time of 216 hrs was applied throughout.

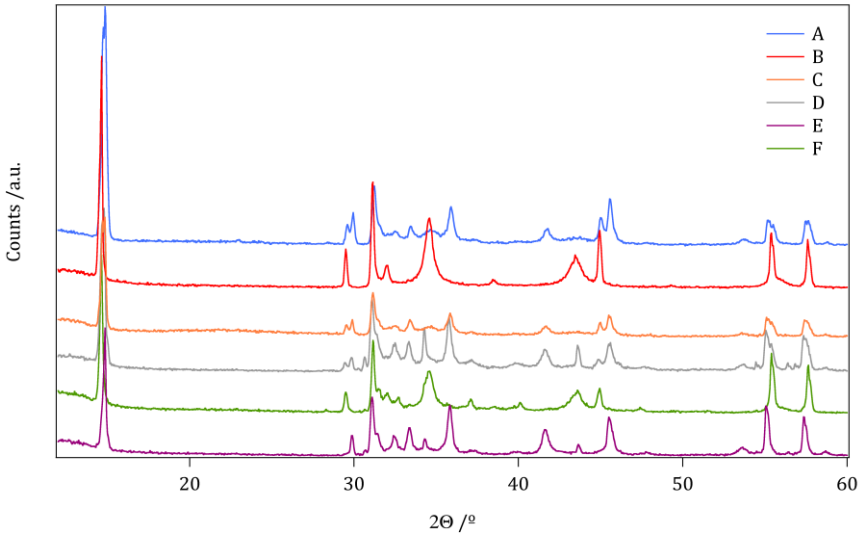

An in depth qualitative analysis of the peak structure of the powder diffraction pattern of **1** (*vide infra*) reveals a mixture of 2H and 6R phases. Indexation of the powder diffraction peaks, by assuming a hexagonal symmetry, yielded unit cell parameters: $a = b = 3.315(1)$, $c = 12.091(6)$ Å, and $\gamma = 120^{o}$ for the 2H component and $a = b = 3.3350(1)$, $c = 35.850(3)$ Å, and $\gamma = 120^{o}$ for the 6R one, both in excellent agreement with that described in the literature for the 2H and 6R polytypes.[1]

[1] A. Meetsma, G. A. Wiegers, R. J. Haange, J. L. de Boer, *Acta. Cryst.* **1990**, *C46*, 1598-1599.

(*Bottom*) XRPD comparison of compound **1** and theoretical powder patterns of two TaS_2 phases.

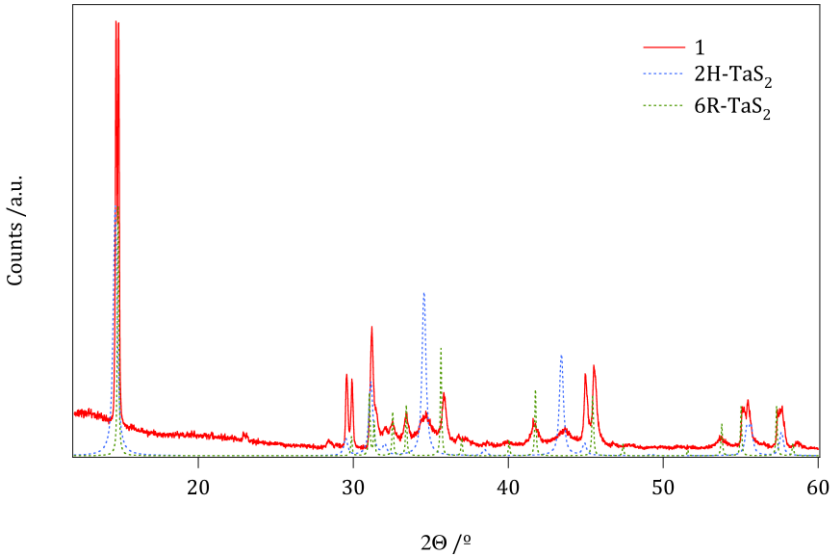

SI 2. SEM studies of alternative TaS_2 batches.

Despite their even morphology, the presence of contaminant phases discarded their use. Picture labels correspond to sample references at SI1.

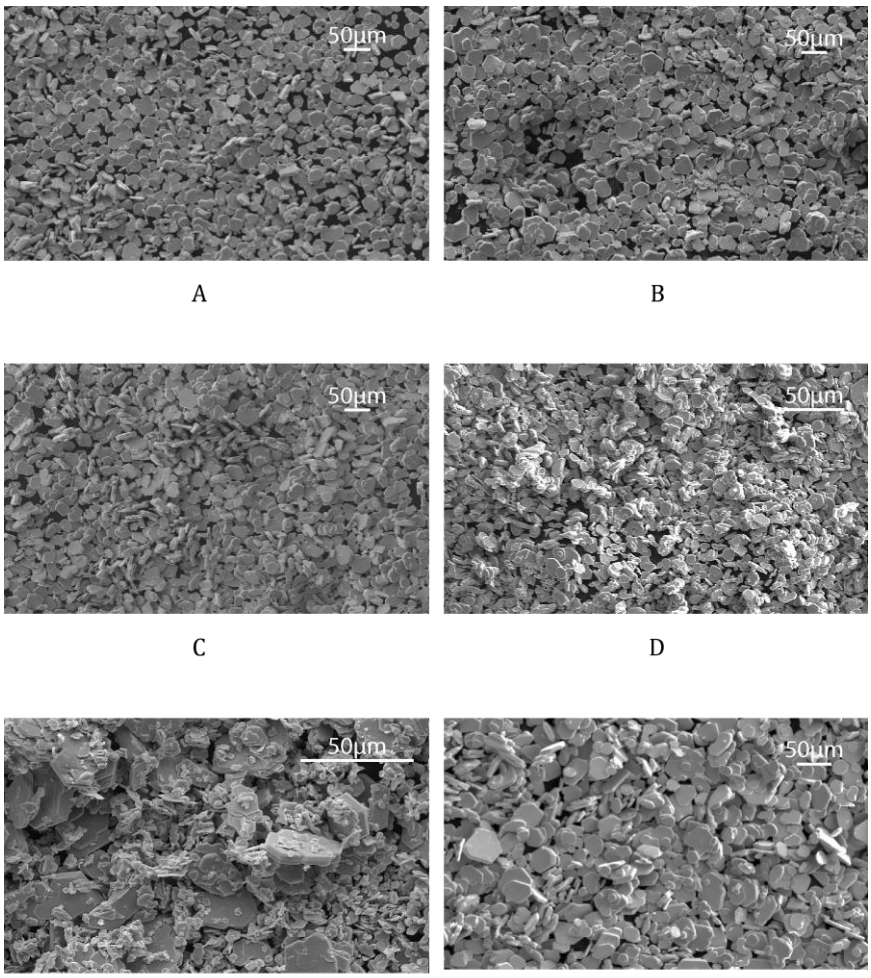

SI 3. Chemical characterization of hybrid samples.

Metallic composition of bulk samples expressed as atomic percentage extracted from energy dispersive spectroscopy (EDAX) studies collected from samples: $Na_{0.33}[TaS_2]$ (**2**), $[Mn_4(OAc)_2(pdmH)_6]_{0.15}[TaS_2]$ (**4**).

	% Ta		% Na		% Mn	
	theor.	*exp.*	*theor.*	*exp.*	*theor.*	*exp.*
2	75.0	76.5	25.0	23.5	-	-
4	60.0	63.5	-	-	40.0	36.5

SI 4. SEM images of the Na^+-intercalated material (**2**).

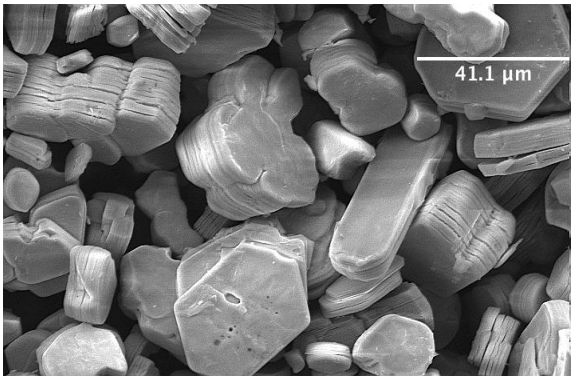

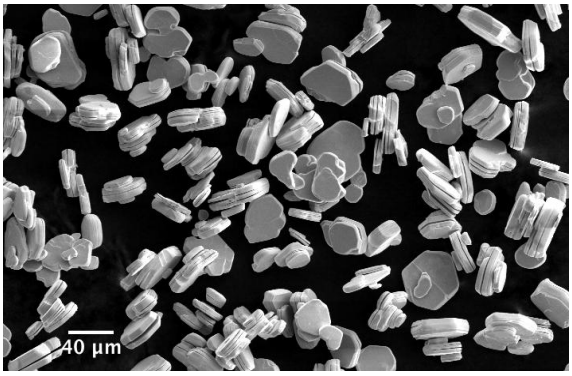

SI 5. FT-IR of the $[Mn_4(OAc)_2(pdmH)_6](ClO_4)_2$ salt (**3**).

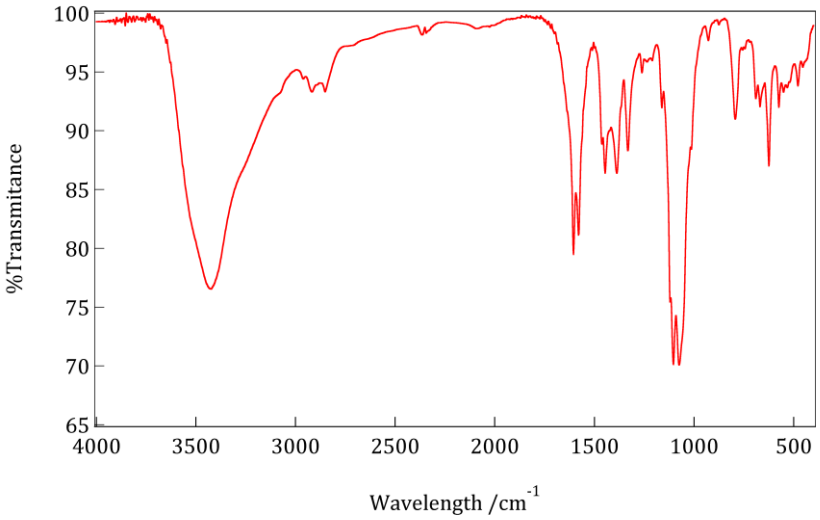

FT-IR (cm^{-1}): 3423,4 (m, br), 2913,1 (w), 2650,7 (w), 1604,5 (m, sh), 1578,3 (m, sh), 1462,4 (m, sh), 1445,8 (m, sh), 1387,0 (m, sh), 1330,6 (m, sh), 1237,7 (w, sh), 1205,0 (w, sh), 1161,0 (w, sh), 1103,6 (st, sh), 1070.9 (s, br), 1008,9 (m, sh), 928,1 (w, sh), 790,5 (m, br), 743,2 (w), 690,7 (m, sh), 669,5 (m, sh), 624,4 (m, sh), 574,0 (m), 547,7 (m), 530,8 (m), 478,9 (m), 453,1 (m), 443,9 (m), 434,5 (m).

[Where: st (strong), m (medium), w (weak); and: broad (br), sharp (sh).]

SI 6. Unit cell parameters comparing literature Mn_4 [2] and acetonitrile/diethyl ether re-crystallized **3**.

Structure	a /Å	b /Å	c /Å	α /º	β /º	γ /º	V /Å^3
Yoo *et al.*	11.914(3)	15.347(4)	9.660(3)	104.58(1)	93.42(1)	106.06(1)	1626
3	11.9510(2)	15.5050(2)	9.7310(2)	105.1880(11)	93.3650(10)	105.8120(11)	1657.82

[2] J. Yoo, E. K. Brechin, A. Yamaguchi, M. Nakano, J. C. Huffman, A. L. Maniero, L.-C. Brunel, K. Awaga, H. Ishimoto, G. Christou, D. N. Hendrickson, *Inorg. Chem.* **2000**, *39*, 3615-3623.

SI 7. Flocculating Mn_4 concentration $[Mn_4(OAc)_2(pdmH)_6](ClO_4)_2$ (mmol per L of acetonitrile) dependency of hybrid **4** stoichiometry studied by EDAX.

$[Mn_4]$ /mM	Molar excess Mn_4	% Ta		% Mn	
		theor.	*exp.*	*theor.*	*exp.*
2.14	x1		63.5		36.5
2.14	x2	60	78.9	40	21.1
3.21	x2		65.9		34.1

SI 8. Thermogravimetric analysis of Na^+-intercalated material **2** and Mn_4 – TaS_2 hybrid material **4** performed in a N_2 atmosphere.

(*Left*) Na^+-intercalated precursor material δ-$Na_{0.33}[TaS_2]\cdot 1.9H_2O$ (**2**) (*Right*) Hybrid material $[Mn_4(OAc)_2(pdmH)_6]_{0.15}[TaS_2]$ (**4**).

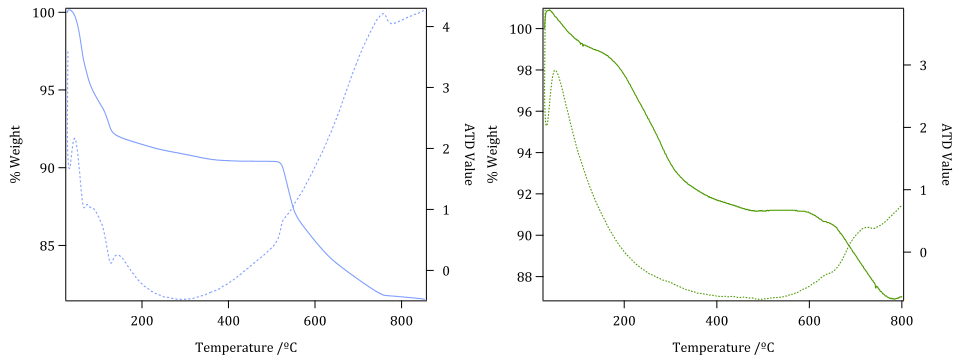

SI 9. Magnetic characterization of precursor material **2**.

Top panels: AC susceptibility (real component to the *left* and imaginary to the *right*) at a fixed frequency of 332 Hz measured at different DC applied field strengths. *Bottom*: (*Left*) Magnetization curve measured at 2 K showing the typical features of a type II superconductor: lower and upper critical fields ($\geq H_{c1}$ and H_{c2}).[3] (*Right*) Magnetization hysteresis loop measured at very low temperatures, showing the effect of vortex pinning.

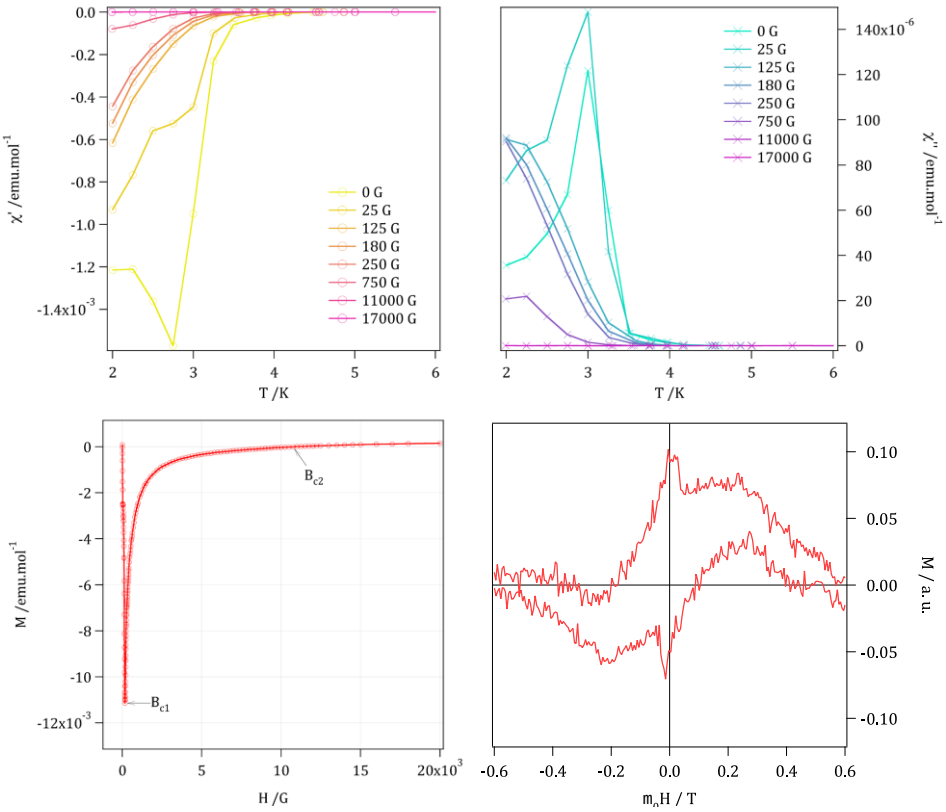

Sample	H_{c1} / Oe	$H_{c2} \cdot 10^{-3}$ / Oe
2	170	10.9

[3] C. P. Poole. *Handbook of superconductivity*, Ed. Academic Press, **2000.** *Chapter 12*.

SI 10. Magnetic susceptibility measurements for compound **3** and **4**.

Real *(left)* and imagin ary *(right)* AC susceptibility components of complexes **3** (*top panels*) and **4** *(bottom panels)* measured above 1.8 K under the action of DC applied magnetic fields of varying strength.

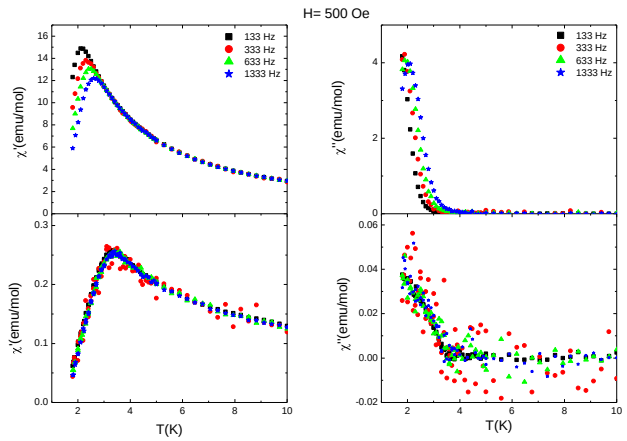

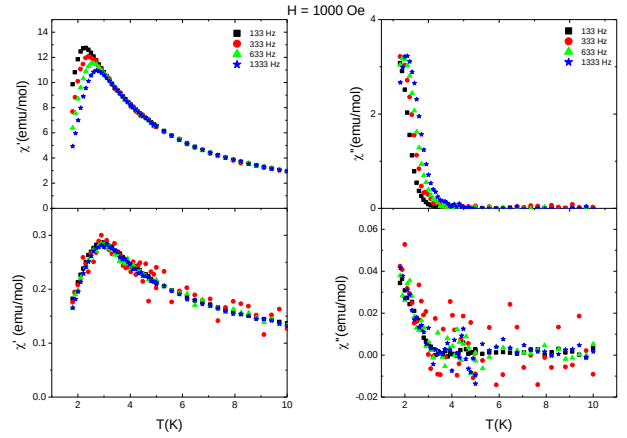

Código de campo cambiado

Código de campo cambiado

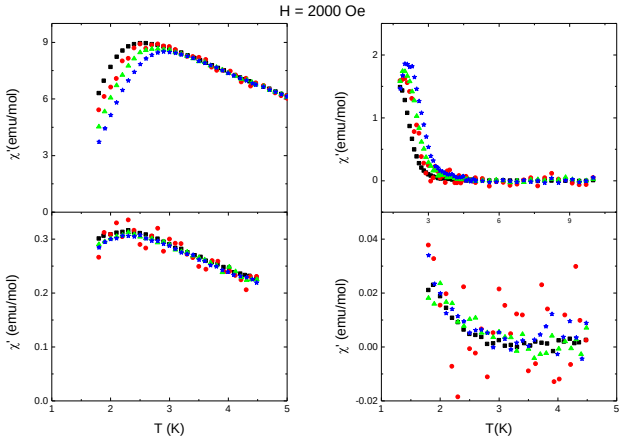

Código de campo cambiado

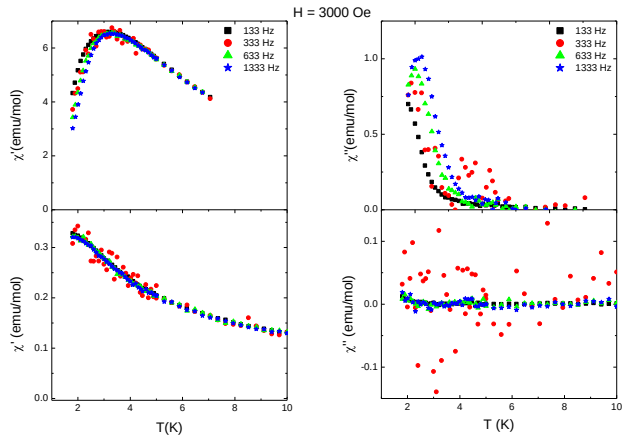

Código de campo cambiado

SI 11. Hysteresis loops of **3** (*top*) and **4** (*bottom*) measured at different temperatures with a μ-Hall sensor. The plots on the right hand side give the coercive field values determined from these loops.

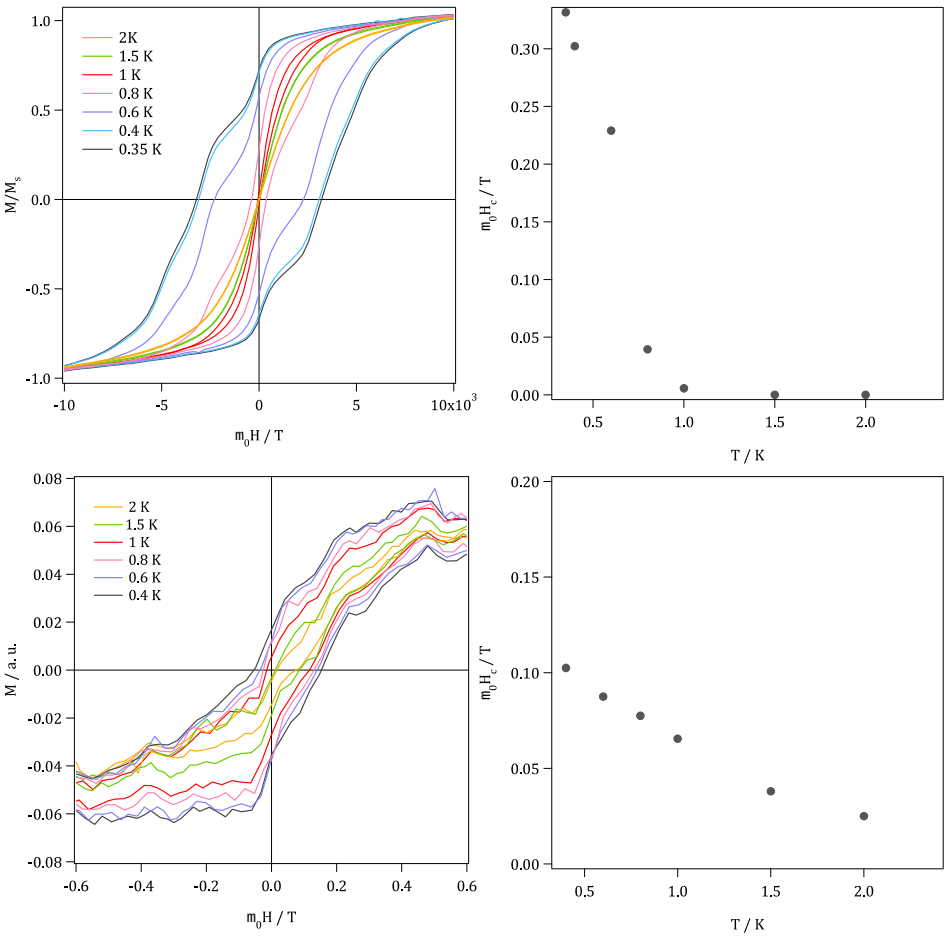

SI 12. SQUID magnetization isotherm curves of the starting material **3** and of the hybrid material **4** at T = 2 and 5 K.

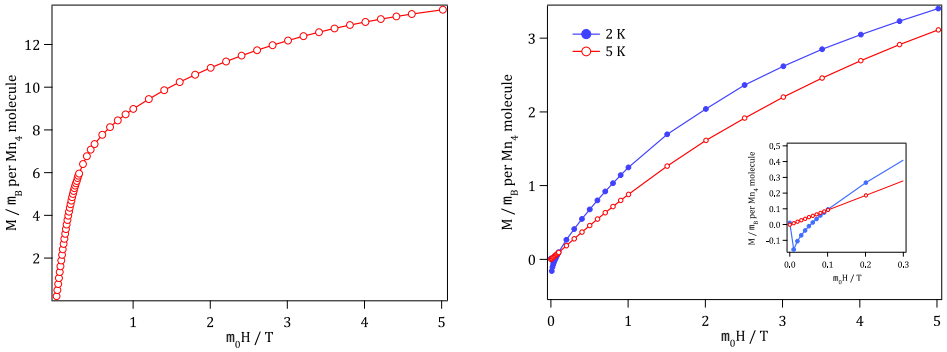

Despite the fact the M does not saturate, even at 2 K, it can be clearly seen that the magnetization measured at the highest field (M(5 T, 2 K) ≈ 3.5 μ_B/Mn_4 cluster) remains much lower than the saturation magnetization (16 μ_B) of complex **3**. Again, this points to a smaller magnetic moment per molecule, exactly as the susceptibility data do. From the initial magnetization curve, the lower critical field H_{c1} of the superconducting fraction can be estimated to be H_{c1} < 200 Oe at T = 2 K, in agreement with the value (170 Oe) found for the precursor material **2**.

SI 13. Magnetic SQUID measurements performed on thin crystallite-oriented pellets of hybrid material **4**.

The macroscopic magnetization is largely determined by the shape of the sample and, in our case of a highly anisotropic superconductor, also by the orientation of the external magnetic field with respect to the TaS_2 planes. Experiments were carried out on oriented samples, pressed in form of very thin pellets where the flat sample faces were approximately parallel to the TaS_2 planes. The magnetization and the ac susceptibility have been measured with the external magnetic fields (AC and DC) either parallel or perpendicular to these faces.

(*Top*) Low temperature magnetization curves for hybrid material prepared in the form of an oriented pellet. Graphs show data for perpendicular (opaque markers) and parallel (transparent) orientations of the pellet relative to the external applied field. *Left*: full profile; *right*: low field region zoom, including ideal Meissner response (solid green line). (*Bottom*) χ_{real} extracted from AC magnetic susceptibility measurements performed on an oriented pellet of hybrid **4**. Measurements were performed in a parallel (||) and perpendicular (⊥) conformation of the pellet with respect to the applied external field. The dotted red line reads the magnetic susceptibility expected if the sample were an ideal diamagnet. *Left*: full profile; *right*: low temperature region showing coincident response for both conformations.

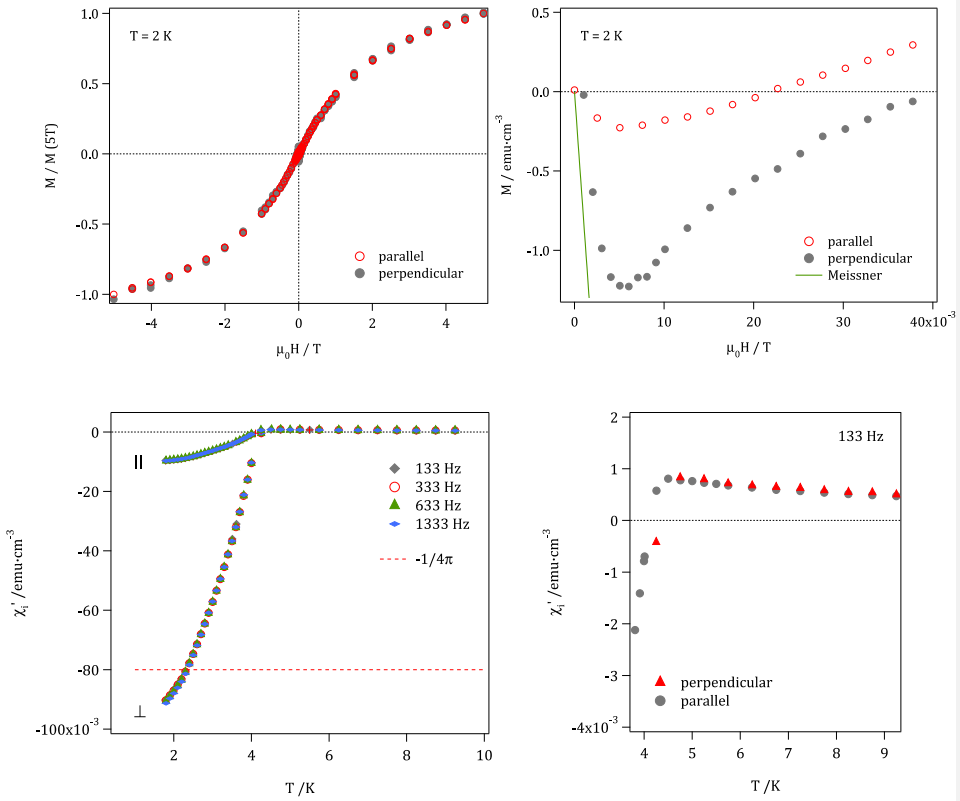

SI 14. XPS studies: binding energy (BE/ eV) and chemical state determination.

Top: Comparison of XPS Mn peaks for pristine $[Mn_4(OAc)_2(pdmH)_6](ClO_4)_2$ sample **3** (*left panels*) and hybrid material **4** (*right panels*). *Bottom*: Mn $2p_{3/2}$, Mn 3s and Mn 3p experimental binding energy estimated values (in eV) and chemical state assignment (*in brackets*) extracted from previous high resolution (narrow) scans.

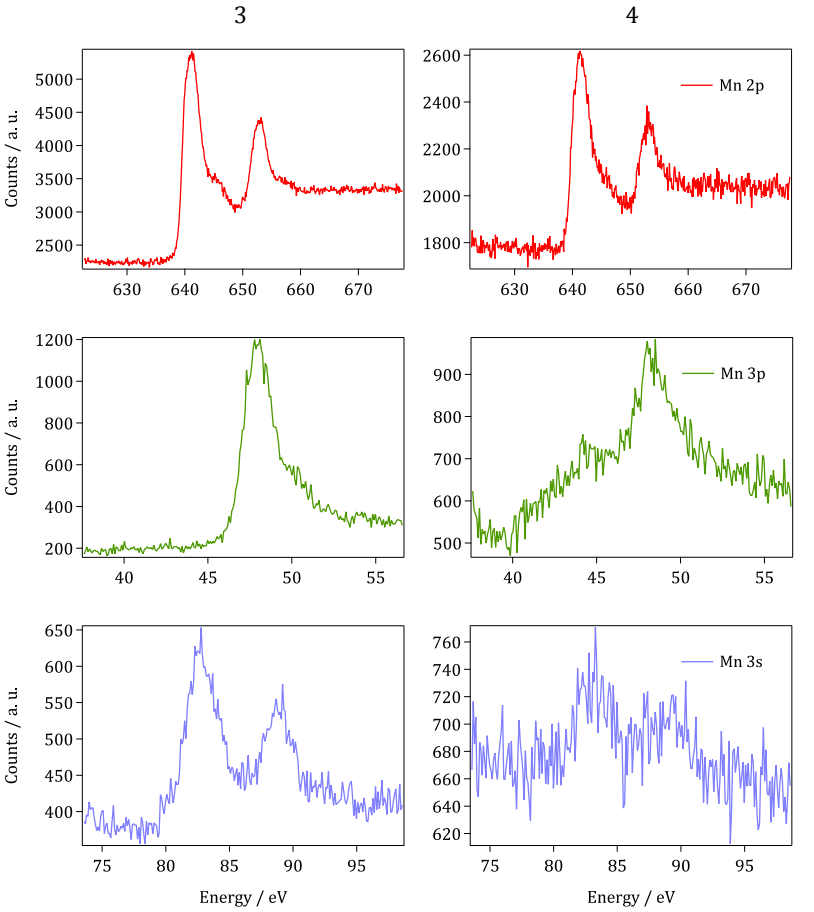

Sample	Mn $2p_{3/2}$	Mn 3s' – Mn 3s''	Mn 3s	Mn 3p
			spin-energy splitting	
3	641.2 (Mn^{2+}) 642.7 (Mn^{4+}) 645.2 (sat. Mn^{2+})	83.3-89.7 84.8-88.9	6.4 (Mn^{2+}) 4.08 (Mn^{4+})	48.64 (Mn^{2+}/ Mn^{3+}) 50.60 (Mn^{4+})
4	641.3 (Mn^{2+}) 642.86 (Mn^{4+}) 645.1 (sat. Mn^{2+})	83.2-90 84.6-88.2	6.7 (Mn^{2+}) 3.6 (Mn^{4+})	48.68 (Mn^{2+}/ Mn^{3+}) 50.0 (Mn^{4+})